Inertial lift on a particle in a straight microchannel of Newtonian, power-law and Carreau-Yasuda fluids: A simulation study toward optimized particle separation

Mehryar Jannesari Ghomsheh, Azadeh Jafari, Denis Funfschilling

▶ **To cite this version:**

Mehryar Jannesari Ghomsheh, Azadeh Jafari, Denis Funfschilling. Inertial lift on a particle in a straight microchannel of Newtonian, power-law and Carreau-Yasuda fluids: A simulation study toward optimized particle separation. Journal of Non-Newtonian Fluid Mechanics, 2023, 312, pp.104977. 10.1016/j.jnnfm.2022.104977 . hal-04275692

HAL Id: hal-04275692
https://hal.science/hal-04275692v1

Submitted on 8 Nov 2023

HAL is a multi-disciplinary open access archive for the deposit and dissemination of scientific research documents, whether they are published or not. The documents may come from teaching and research institutions in France or abroad, or from public or private research centers.

L'archive ouverte pluridisciplinaire **HAL**, est destinée au dépôt et à la diffusion de documents scientifiques de niveau recherche, publiés ou non, émanant des établissements d'enseignement et de recherche français ou étrangers, des laboratoires publics ou privés.

Inertial Lift on a Particle in a Straight Microchannel of Newtonian, Power-law and Carreau-Yasuda Fluids: A Simulation Study Toward Optimized Particle Separation

Mehryar Jannesari Ghomsheh[1,2], Azadeh Jafari[1,3, a)], Denis Funfschilling[3, a)]

[1]School of Mechanical Engineering, Faculty of Engineering, University of Tehran, P.O. Box 11155-4563, Tehran, Iran

[2]Robert Frederick Smith School of Chemical and Biomolecular Engineering, Cornell University, Ithaca, NY, 14853, USA

[3]Université de Strasbourg, CNRS, ICube UMR 7357, 2, Rue Boussingault, F-67000 Strasbourg, France

[a)]Authors to whom correspondence should be addressed: azadeh.jafari@ut.ac.ir, dfunfschilling@unistra.fr

Abstract

Direct three-dimensional Numerical Simulations (DNS) are performed to calculate the inertial lift forces on a single particle in a straight rectangular microchannel of Newtonian fluid and xanthan gum solutions. The shear-thinning behavior of xanthan gum solutions is demonstrated experimentally and represented mathematically using the power-law and Carreau-Yasuda models. Similar to Newtonian fluids, our simulations delineate the dominant region of shear gradient and wall-induced lift forces for power-law and Carreau-Yasuda fluids. The variable viscosity of non-Newtonian fluids allows us to better control the particle motion which seems promising in the inertial focusing method. Owing to their different formulations, power-law and Carreau-Yasuda models result in inconsistent lift forces. This incompatibility appears to intensify at higher concentrations of xanthan gum (higher shear-thinning characteristics) solutions and stems from the fact that the power-law viscosity considerably diverges from the experimental and Carreau-Yasuda viscosity in both low and high shear-rate regions. The power-law model is more sensitive to the Re number compared to the Carreau-Yasuda model, especially for high concentrations of xanthan gum solutions. Furthermore, the results indicate the presence of two equilibrium positions for both Newtonian fluid and xanthan gum solutions in the microchannel cross-section. By increasing the Re number, the Newtonian and Carreau-Yasuda fluids push the particle equilibrium positions toward the center of the microchannel while the power-law model pushes the equilibrium positions toward the microchannel wall. Furthermore, both power-law and Carreau-Yasuda models indicate the shift of equilibrium positions to the microchannel wall by increasing the shear-thinning characteristics.

Key words: Particle separation, Inertial microfluidics, Inertial lift forces, Newtonian fluid, Power-law model, Carreau-Yasuda model

1 Introduction

With its improved portability, high efficiency and throughput, and low costs, microfluidic technology has outperformed all other particle separation platforms (e.g., centrifuge, flow cytometry, etc.) in recent years [1]. Inertial microfluidics is the intermediate regime between the Stokes regime and the turbulent regime, where both inertial and viscous forces are comparable. Inertial migration and secondary flow are the fundamental elements of inertial microfluidics that account for its striking characteristics [2]. Inertial migration, which was primarily observed by Segre and Silberberg [3], is the lateral movement of randomly dispersed particles to several equilibrium positions in a straight microchannel. Following this observation, numerous articles in the literature have suggested the underlying reasons for this phenomenon [4–9].

Generally, the final lateral position of the particles in a straight microchannel is pinpointed by the balance of four different lift forces exerted on the particle: (1) Saffman force, which results from velocity gradient in a simple shear flow [10], (2) Magnus force, which only acts on rotating particles in a fluid [11], (3) wall-induced lift force, which repels the particles away from the wall [12], and (4) shear gradient lift force, which arises from the curvature of the velocity profile [13]. Saffman and Magnus forces are usually negligible for particles immersed in a Poiseuille flow. Shear gradient lift force pushes the particles toward the wall, while wall-induced lift force repels them. The balance between these forces creates four and two equilibrium positions in a straight microchannel with square cross-section and rectangular cross-section, respectively [14].

Analytical studies have been conducted to calculate the lift forces on a small sphere using perturbation methods to solve Navier-Stokes equations, but they were limited to low Reynolds (Re) numbers [15–17]. Ho and Leal [18] explained the focusing pattern in tube flows and derived an explicit formula for the lift force in low-Re-number flows. Di Carlo et al. [19] introduced position-dependent scaling for the inertial lift in microchannels by defining two different scales for particles near the channel center and near the channel wall, but these scales were limited to straight square microchannels. Liu et al. [20] conducted experimental and numerical simulations to predict the inertial lift forces on a single particle in a Newtonian fluid over a wide range of Re numbers, and based on these results, they derived a generalized formula, which is applicable for certain ARs and Re numbers, for calculating the inertial lift on a sphere in a microchannel [21]. Similarly, Mashhadian and Shamloo [22] predicted the focusing pattern of particles in a straight microchannel with different cross-sections based on

the numerical results of the lift force of a Newtonian fluid on a particle in a rectangular microchannel. Furthermore, the advent of machine learning algorithms has enabled researchers to accurately predict the inertial lift forces on the particles in Newtonian fluids due to a wide range of available databases of these fluids [23].

Unlike Newtonian fluids, inertial focusing of particles and cells in non-Newtonian fluids is not studied thoroughly and thus requires further examinations. The use of non-Newtonian fluids allows for better control of particle motion due to their rheological characteristics, ranging from shear-thinning to plastic and elastic behaviors [24–28]. Hu et al. [29] determined the effects of Re number, power-law index, and blockage ratio on the particle trajectory in a two-dimensional Poiseuille flow of a power-law fluid using immersed boundary-lattice Boltzmann method and showed that an increase in the power-law index and the blockage ratio and a decrease in the Re number reduces the particle spacing. In a similar study [30], they incorporated the effects of microchannel AR into their previous results and found different particle trajectories in three-dimensional straight microchannels. They observed that the equilibrium positions in a straight microchannel move toward the center by increasing the power-law index and the blockage ratio and decreasing the Re number, and this pattern does not change with the microchannel AR. Chrit et al. [31] investigated the role of particle elasticity in its final equilibrium position in the Poiseuille flow of shear-thinning and shear-thickening fluids. According to their results, the particle elasticity does not exert a decisive effect on the final equilibrium position, especially for small capillary (Ca) numbers. Hu et al. [32] determined the effect of the particle shape on its final equilibrium position in a channel flow of power-law fluids. Their results show that the shortest distance between the initial position and the equilibrium position is achieved for the rectangular particle, then followed by elliptical, circular, and square particles, respectively. Based on the mentioned studies, the shear-thinning and shear-thickening behaviors shift the equilibrium position of the particle toward the wall and center of the microchannel, respectively [29–32].

As mentioned previously, the particle focusing in microfluidics has attracted a great deal of attention during the past years. There are multiple factors, like the microchannel geometry, particle size and shape, flow rate, rheological characteristics of the fluid, among others determining the behavior of the particle in microfluidics. To study these complex dynamics, there are two general approaches; first, one can release the particle in the flow and track its movement based on the forces exerted on the particle. The second approach, on the other hand, treats the particle as a stationary obstacle in the flow and aims to solve the flow around it. The

first approach provides the particle trajectory toward its equilibrium position and the time required to reach the equilibrium position. In contrast, the second approach cannot grant the history of the particle movement in the microchannel but can calculate the inertial lift forces exerted on it. Although the equilibrium position of different particles in Newtonian and power-law fluids with different Re numbers has been extensively studied with the first approach, to the best of our knowledge, the magnitude of inertial lift forces is not calculated for a particle in a non-Newtonian fluid, especially in moderate and high Re numbers. Obtaining the dependence of inertial lift forces on the mentioned factors will deepen our understanding of particle dynamics and facilitate future studies in this direction. As a concrete example, by having these forces, an enormous amount of computational cost is reduced, and one can easily simulate the particle separation in curved microchannels by integrating the obtained inertial lift forces into the Lagrangian tracking method for each cross-section and Re number. This approach relies on the fact that the channel bends produce a minimal effect on the lift force but a significant effect on the secondary drag force, so these two forces can be analyzed separately [33–37].

In this paper, a numerical simulation of inertial lift forces exerted on a single particle in a straight microchannel with a rectangular cross-section is carried out for a Newtonian fluid and xanthan gum solutions at two different Re numbers, and the results are interpreted. Xanthan gum solutions are frequently employed for the purpose of particle separation and as viscosity thickener in the food processing industry [38–42]; however, this is the first time in the literature that the inertial lift forces are calculated for a particle in these solutions. The choice of these solutions is due to their strong shear-thinning characteristics, which can trigger the emergence of rich phenomena in particle migration. For this purpose, two different xanthan gum solutions are experimentally tested, and the power-law and Carreau-Yasuda models are used for the prediction of their behavior, and viscosity fitting results and the calculated lift forces are compared. The results of the present study not only can serve as a benchmark for calculating the inertial lift forces on the particles in non-Newtonian fluids but also, as discussed earlier, can be beneficial for obtaining particle trajectory even in curved microchannels. Furthermore, the obtained results can be used in particle and cell separation in many biological fluids, such as blood, due to their shear-thinning characteristics, which can be represented by the Carreau-Yasuda model for different Hematocrit (Hct) percentages [43].

2 Xanthan Gum Preparation

Xanthan gum solutions are strongly shear-thinning fluids with small normal stress differences and are frequently used in industrial applications [44–46]. Two solutions of xanthan gum (Rhodigel USP, viscosity of $0.876\ Pa.s$ at $24°C$ at a concentration of 1%) of 300 and 500 ppm were prepared by introducing the xanthan gum in distillated water and gently stirring the solutions with a helical ribbon for 24 hours. The viscosities of these solutions were measured on an AR2000 rheometer (TA Instruments) with a $60mm$ steel cone of 1° angle by a steady-state point by point measurement.

3 Mathematical Modeling and Numerical Procedure

In this part, the 3D DNS procedure for the calculation of the inertial lift force is stated. The continuity, momentum, and constitutive equations are numerically solved based on an iterative algorithm through the coupling of a FEM solver with a MATLAB code.

3.1 Case Study

The schematic of the particle in the microchannel and the geometrical characteristics are presented in Fig. 1 and Table 1, respectively. A straight rectangular microchannel with a high aspect ratio is used, and the particle is placed far from the inlet and outlet of the microchannel.

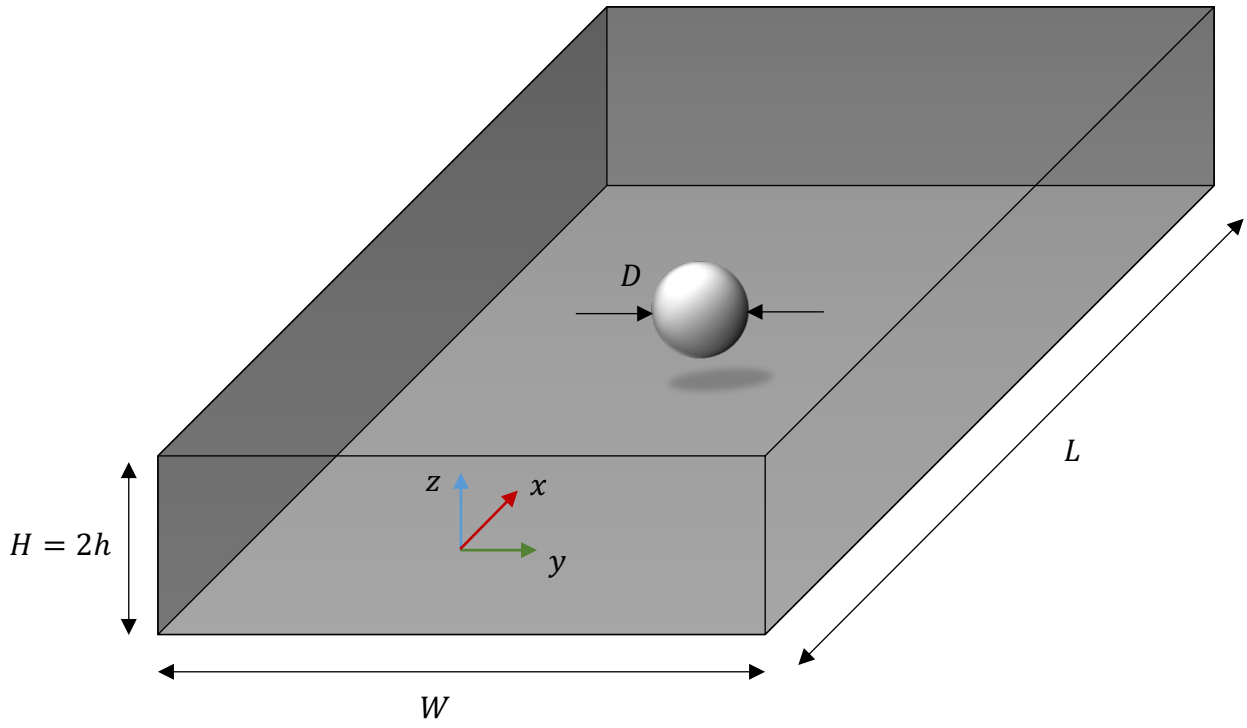

Fig. 1: Schematic of the microchannel with a single particle

Table 1: Geometrical characteristics of the microchannel and the particle

Geometrical Parameter	Value (μm)
Channel Height (H)	48
Channel Width (W)	200
Channel Length (L)	300
Particle Diameter (D)	10

The simulations are carried out for a Newtonian fluid with constant viscosity of $\mu = 0.001\ Pa.s$ and the two mentioned xanthan gum solutions as non-Newtonian fluids. To correctly represent the behavior of xanthan solutions, the non-Newtonian model must have a defining shear-thinning characteristic. As a result, the power-law and Carreau-Yasuda models are used in this study. The general form of Ostwald and de Waele power-law model [47] can be represented as follows:

$$\eta = m \left| II_{\underline{\underline{\dot{\gamma}}}} \right|^{\frac{(n-1)}{2}} \tag{1}$$

where η is the fluid dynamic viscosity, m is the consistency index, n is the power-law index, and $II_{\underline{\underline{\dot{\gamma}}}}$ is the second invariant of the rate of strain tensor, $\underline{\underline{\dot{\gamma}}}$, and is defined as

$$II_{\underline{\underline{\dot{\gamma}}}} = \frac{1}{2}\left[\left(tr\underline{\underline{\dot{\gamma}}}\right)^2 - tr\left(\underline{\underline{\dot{\gamma}}}\right)^2\right]. \tag{2}$$

For simple shear flows, the absolute value of the second invariant becomes:

$$|II_{\underline{\underline{\dot{\gamma}}}}| = \left|\underline{\underline{\dot{\gamma}}}\right|^2 \tag{3}$$

and thus simplifies the power-law model to the popular form of

$$\eta = m \left|\underline{\underline{\dot{\gamma}}}\right|^{n-1}. \tag{4}$$

This model can represent the shear-thinning behavior with great accuracy in intermediate shear-rate regions but is not able to display the shear-thinning characteristics of fluids in the near-zero or infinite shear-rate regions. To overcome this problem, the well-known Carreau-Yasuda model [48] is used as well, in which the fluid viscosity is expressed as follows:

$$\eta = \eta_\infty + (\eta_0 - \eta_\infty)\left[1 + \left(\lambda \left|II_{\underline{\underline{\dot{\gamma}}}}\right|^{1/2}\right)^a\right]^{\frac{n_{CY}-1}{a}} \quad (5)$$

where η_∞ is the infinite shear-rate viscosity, η_0 is the zero shear-rate viscosity, λ is a time constant, n_{CY} is the power-law index, and a is a dimensionless fitting parameter introduced by Yasuda et al. [48]. Furthermore, all simulations are repeated for two different Re numbers of 48 and 90, a constant fluid density of $\rho_f = 1000\, kg/m^3$, and particle density of $\rho_p = 1050\, kg/m^3$.

3.2 Inertial Lift Force Calculation

The total inertial lift force is a function of microchannel geometry, particle diameter, and the shape of the velocity profile and can be expressed as follows:

$$F_L = F\,(D, y, z, H, W, V_c, \eta, \rho_f) \quad (6)$$

where y and z are the positions of the center of the particle in the microchannel cross-section and V_c is the characteristic velocity of the fluid. Using the Buckingham Pi theorem, the non-dimensional form of the inertial lift force is

$$F_L^* = F\,(\kappa, y^*, z^*, AR, Re) \quad (7)$$

where $\kappa = \frac{D}{H}$ is the blockage ratio, $y^* = \frac{y}{H}$ and $z^* = \frac{z}{H}$ are the non-dimensional position of the particle, AR is the aspect ratio of the microchannel, and Re is the Re number of the flow, generally defined as $Re = \frac{\rho V_c L_c}{\eta_c}$, where L_c and η_c are the characteristic length and characteristic viscosity of the fluid, respectively [49]. The characteristic values should be selected in a way to represent the fluid behavior. There are several definitions of the Re number based on these characteristic values, two of which are shown in Table 2 for Newtonian and power-law fluids. It is worth mentioning that, except for some simplified models [50–52], there is no comprehensive Re number for Carreau-Yasuda constitutive equation. Thus, to be more consistent with the power-law model, the Re number is considered the same for the power-law and Carreau-Yasuda models. In addition, one can also use the local values of mentioned parameters to obtain the local Re number of the flow [53].

Table 2: Different definitions of characteristic values for the calculation of Re number

Fluid model	Characteristic velocity, V_c	Characteristic viscosity, η_c	Characteristic length, L_c
Newtonian [2,54,55]	Maximum velocity, U_{max}	Newtonian viscosity, μ	D_h

Power-law [29,56,57]	Mean velocity, U_0^{2-n}	Consistency index, m	D_h^n

Moreover, the inertial lift force can be expressed as a function of the non-dimensional lift coefficient C_L as

$$F_L = C_L \rho_f V_c^2 D^2 \kappa^2. \quad (8)$$

The inertial lift forces are calculated based on a popular iterative approach in which the particle is considered an obstacle that can only have free rotational motion [36,58,59]. Due to the symmetry, the lift forces are only calculated for the particle in the upper half of the short wall. Furthermore, the torque-free condition and the force-free condition in the flow direction are considered the equilibrium state of the particle. The particle velocity in the flow direction is taken into account by moving the flow and the microchannel walls. For this purpose, laminar inflow and outflow boundary conditions are prescribed for the inlet and outlet of the microchannel, respectively with a velocity of $\bar{V} - V_p(t)$, and the walls of the microchannel are considered moving with a velocity of $-V_p(t)$, which $\bar{V}$ and $V_p(t)$ are the mean velocity of the inlet flow and the time-dependent velocity of the center of the particle, respectively. Also, a slip velocity of $\vec{\omega} \times \vec{r}$ is set for the particle surface, which $\vec{\omega}$ and $\vec{r}$ are the vector of angular velocity and the vector of surface position of the particle with respect to its center, respectively.

The momentum and continuity equations for a generalized Newtonian fluid and a three-dimensional incompressible flow with no external forces are as follows:

$$\nabla . \vec{V} = 0 \quad (9)$$

$$\rho_f \left(\frac{\partial \vec{V}}{\partial t} + \vec{V} . \nabla \vec{V} \right) = -\nabla p + \nabla . \underline{\underline{\tau}} \quad (10)$$

$$\underline{\underline{\tau}} = \eta \underline{\underline{\dot{\gamma}}} \quad (11)$$

$$\underline{\underline{\dot{\gamma}}} = (\nabla \vec{V}) + (\nabla \vec{V})^T \quad (12)$$

where $\vec{V}$ is the fluid velocity, p is the pressure, and $\underline{\underline{\tau}}$ is the stress tensor. In addition, Newton's second law of motion governs the forces $\vec{F}$ and torques $\vec{M}$ exerted on the particle:

$$\sum \vec{F} = \int \left(-pI + \underline{\underline{\tau}} \right) . \hat{n} ds \quad (13)$$

$$\sum \vec{M} = \int (\vec{x} - \vec{x}_c) \times \left(-pI + \underline{\underline{\tau}} \right) . \hat{n} ds \quad (14)$$

where I is the identity matrix, $\hat{n}$ is the unit normal vector at the particle surface, $\vec{x}$ is the position of the particle surface, and $\vec{x}_c$ is the position of the center of the particle. The initial values of the particle's translational and angular velocities are set to zero. Then, after solving the governing equations of the flow, the force and torque distribution around the particle are obtained, and the particle velocity is updated as below:

$$u_p^{new} = u_p^{old} + \frac{F_x \times \Delta t}{m_p} \tag{15}$$

$$\vec{\omega}_p^{new} = \vec{\omega}_p^{old} + \frac{M \times \Delta t}{I_p} \tag{16}$$

where Δt is the time step considered $1\mu s$ in this study, m_p is the particle mass, and I_p is the moment of inertia of the particle. This process continues until the equilibrium state of the particle is reached in which the values of the forces and torques exerted on the particle find their final values, satisfying the force-free condition in the flow direction and torque-free condition, respectively. This condition is fulfilled when the absolute value of the force in the flow direction, i.e., $|F_x|$, becomes less than $1.5 \times 10^{-11} N$, and the absolute value of the torques exerted on the particle in y and z directions, i.e., $|M_y|$ and $|M_z|$, become smaller than $1 \times 10^{-18}\ N.m$. [36]. Finally, the last value of the lateral force is considered as the inertial lift force on the particle in the corresponding position. By changing the position of the particle and repeating the same procedure, the range of inertial lift forces across the microchannel cross-section is obtained. The flowchart in Fig. 2 concludes the mentioned algorithm. The generalized minimal residual (GMRES) iterative method is used as the solver with the Incomplete Lower-Upper (ILU) preconditioner to reduce the number of iterations (time steps). In addition, a second order of accuracy is considered for solving the velocity field in the domain. The simulations are validated by comparing our numerical results with the results from Liu et al. [21] The details of this validation along with a mesh dependence study to verify the accuracy of the results are provided in the validation section. Fig. 3 depicts a sample of mesh configuration utilized in the simulations. An optimized mesh is generated which is finer around the particle and coarser away from the particle to increase the accuracy of the results and reduce the computational time simultaneously. It is worth mentioning that to obtain the equilibrium positions along the short axis, all the inertial lift forces are calculated at $y = 0$.

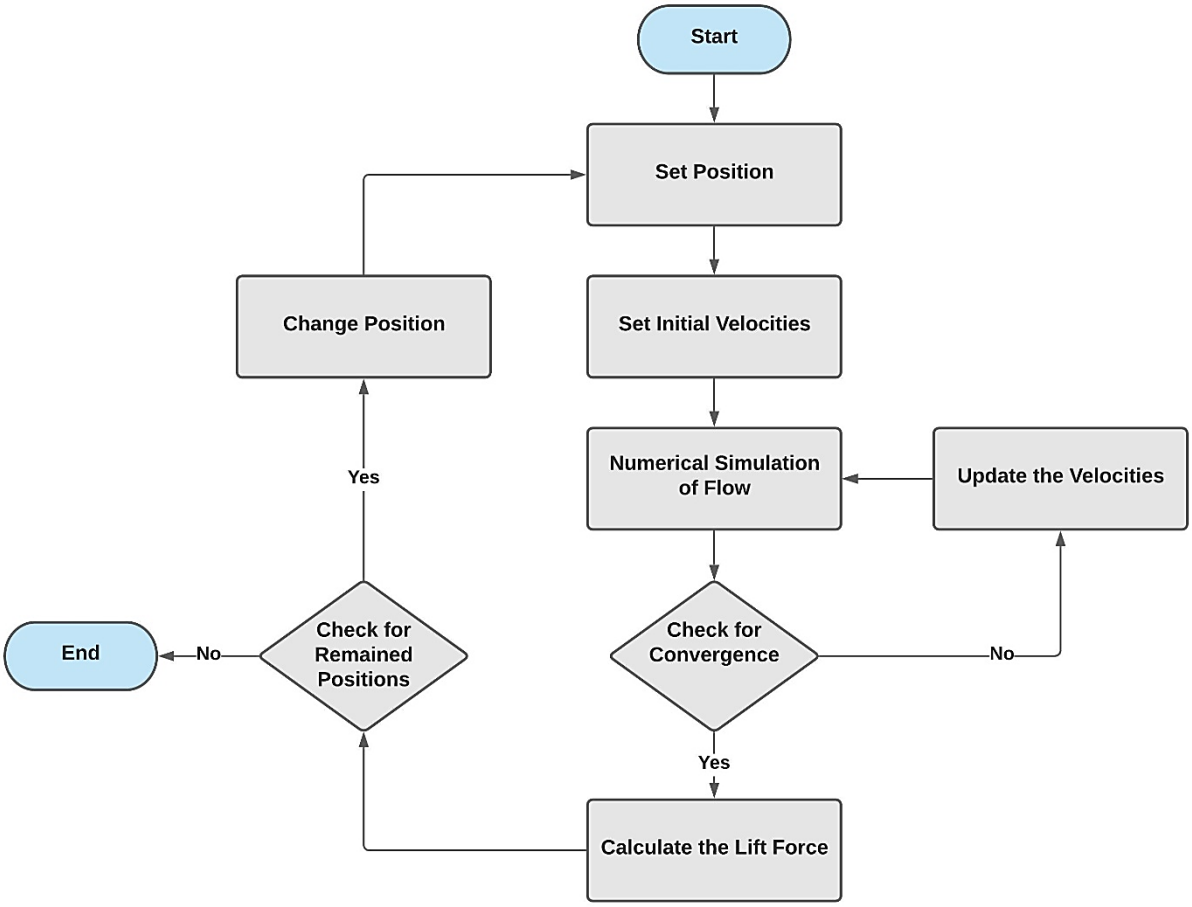

Fig. 2: Flowchart of the inertial lift force calculation

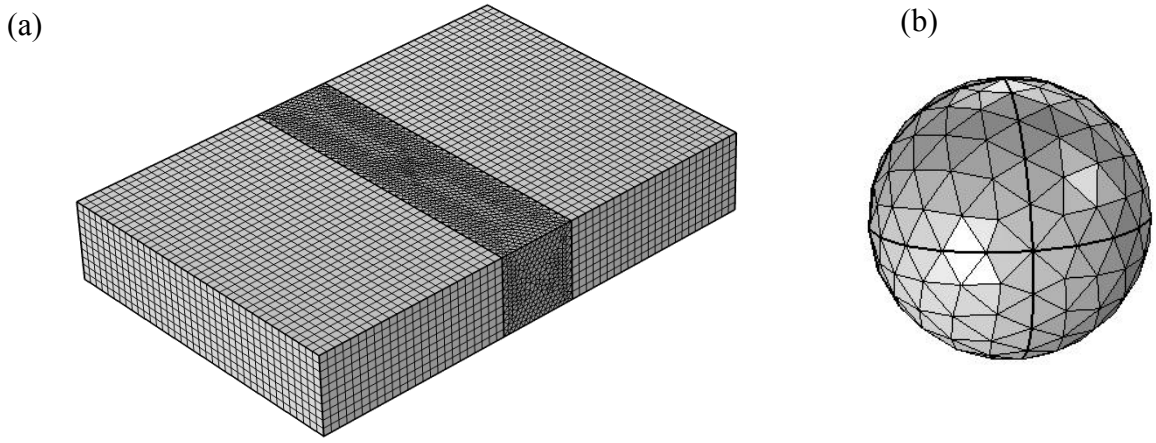

Fig. 3: Sample mesh configuration of (a) microchannel and (b) particle

4 Results and Discussion

In this part, the results are obtained for different meshes and validated by the literature. The power-law and Carreau-Yasuda parameters are obtained based on the experimental viscosity of xanthan gum solutions. Then, the values of inertial lift forces as a function of the particle

position as well as the final equilibrium positions are reported and compared for different viscosity models.

4.1 Validation

The results are validated by the lift formula proposed by Liu et al. [21] for a single particle with a diameter of $D = 15\ \mu m$ in a square straight microchannel with a side of $50\ \mu m$ and a length of $300\ \mu m$. This widely used formula includes the four different inertial lift forces, i.e., Saffman force, Magnus force, wall-induced lift force, and shear gradient lift force, and is obtained by fitting the proposed formula to DNS solutions. Also, a mesh dependence study is carried out to check the accuracy of the results. The selected meshes for this section are presented in Table 3. It was observed that decreasing the size of elements around and far from the particle has negligible effects on the results.

Table 3: Selected meshes for the mesh dependence study

Parameter	Coarse Mesh	Medium Mesh	Fine Mesh
Maximum element size on the particle surface	$2.65\ \mu m$	$1.15\ \mu m$	$0.65\ \mu m$
Maximum element size around the particle	$2.65\ \mu m$	$2.65\ \mu m$	$2.65\ \mu m$
Maximum element size far from the particle	$5\ \mu m$	$5\ \mu m$	$5\ \mu m$
Total number of elements	102636	137590	252765

Fig. 4 draws the comparison between the obtained results and the lift formula proposed by Liu et al. [21] Since the results of the coarse mesh differ considerably from Liu's lift formula, it is not repeated for other points in the microchannel cross-section. The medium mesh correctly matches Liu's lift formula. The consistency between the fine mesh and the medium mesh results verifies the validity of the medium mesh for simulations. The medium grid size can capture the lift forces around the particle with acceptable accuracy, so it is selected as the optimal grid size in the study.

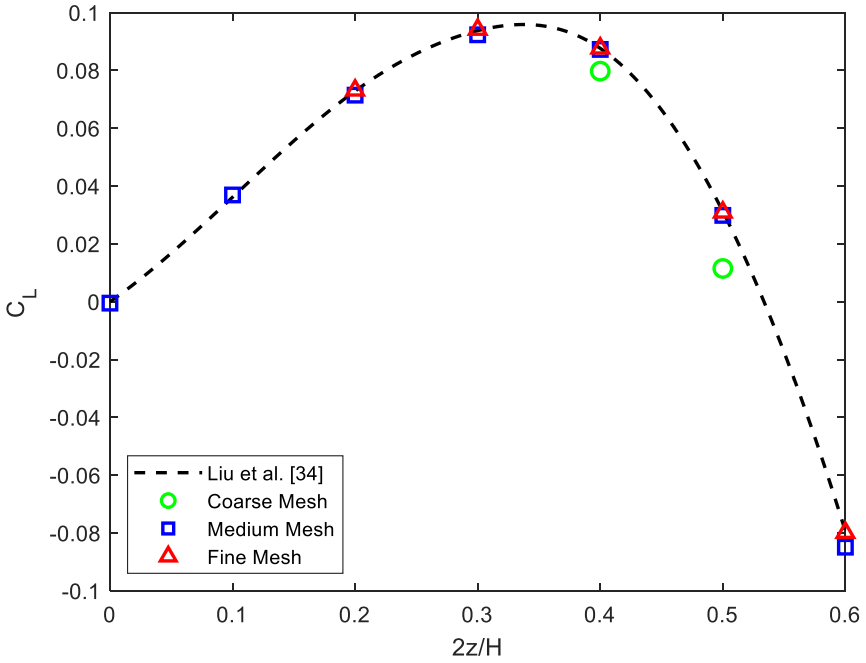

Fig. 4: Lift coefficient for different meshes compared with Liu's formula for the test geometry

4.2 Convergence Results

Based on the procedure adopted for the calculation of the inertial lift forces, a convergence history for dependent variables can be obtained (Fig. 5). At the beginning of the calculations, due to the initial assumption of the variables, the error values of the calculations are high in the first iterations. Then, errors in the calculations sharply decrease and meet the convergence criteria. These errors are calculated based on the differences in the parameters between the two consecutive iterations. As the number of iterations increases, the variation of each parameter decreases resulting in a decrease in the error values of each parameter. Needless to say, the convergence history varies with particle position, the Re number of the flow, and the viscosity model.

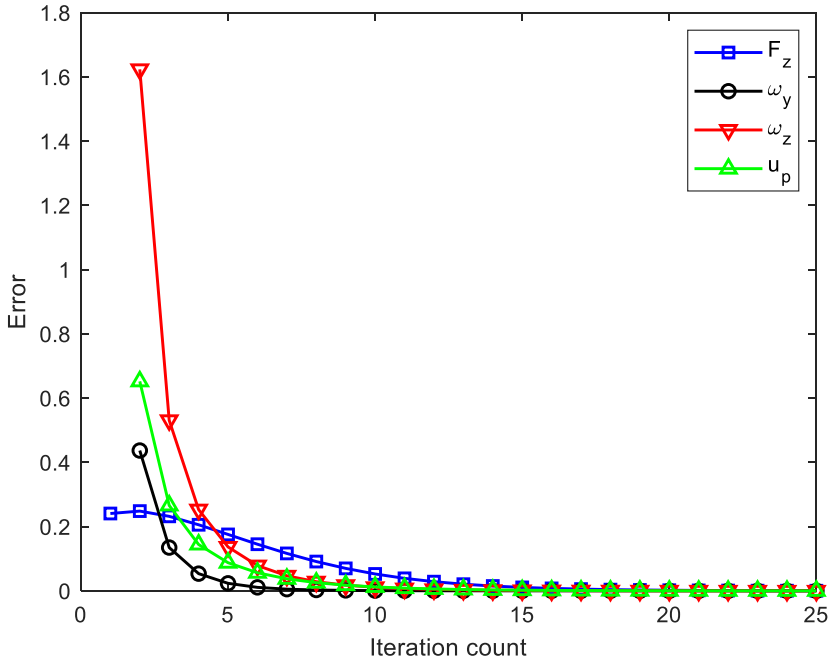

Fig. 5: Convergence history of inertial lift and velocity components (sample case: Newtonian fluid, $Re = 90, \frac{2z}{H} = 0.7$)

4.3 Xanthan Gum Viscosity

By fitting different parameters in both power-law and Carreau-Yasuda models, the viscosity of xanthan gum solutions with different concentrations can be represented mathematically. Table 4 shows the fitting results and the parameters obtained from the two non-Newtonian models to show the behavior of xanthan gum solutions. The power-law representation shows stronger shear-thinning behavior for higher concentrations, which is in agreement with previous results [38]. Furthermore, the Carreau-Yasuda model converges to the original Carreau model ($a = 2$) for the higher concentration of xanthan gum solution. Fig. 6 shows the prediction of xanthan gum viscosity with Carreau-Yasuda and power-law models for 300 ppm and 500 ppm concentrations on a logarithmic scale. As expected, the power-law model cannot accurately capture the xanthan gum viscosity at low and high shear rates, but the Carreau-Yasuda model accurately describes the viscosity over the entire range of shear rates. More specifically, in theory, the power-law model overpredicts and underpredicts the viscosity in the low and high shear-rate regions, respectively. However, we were not able to test the xanthan gum solutions at very low shear rates due to the limitations of the rheometer, but by extending the experimental data to lower shear rates, the power-law model loses its validity to represent the zero shear-rate viscosity. On the other hand, the range of flow rates studied in this study lies

within intermediate and high values of shear rates (greater than 1 s^{-1}), so there is no need to extend the power-law and Carreau-Yasuda viscosities to infinitesimal shear rates.

Table 4: Power-law and Carreau-Yasuda fitting results for xanthan gum solutions

Fluid	Power-law		Carreau-Yasuda				
	$m\ (Pa.s)$	n	$\eta_0(Pa.s)$	$\eta_{inf}\ (Pa.s)$	$\lambda\ (s)$	n_{CY}	a
Xanthan gum solution – 300 ppm	0.0320	0.6805	0.0703	0.0020	0.2079	0.2392	0.3968
Xanthan gum solution – 500 ppm	0.0685	0.5027	0.6491	0.0016	49.70	0.4303	1.9900

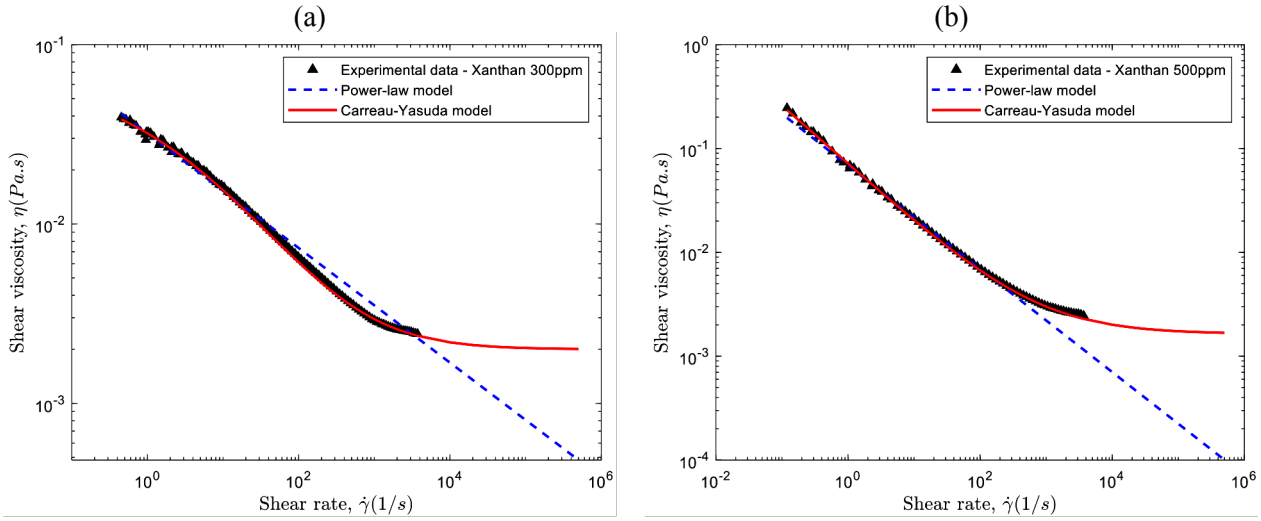

Fig. 6: Experimental and fitting viscosity of (a) 300 ppm and (b) 500 ppm xanthan gum solution as a function of shear rate

4.4 Inertial Lift Forces

Fig. 7 represents the coefficient of inertial lift forces as a function of the particle position for two different Re numbers of the Newtonian fluid. The equilibrium position of the particle can be considered as the one where the inertial lift forces exerted on the particle change direction, i.e., become zero. Consequently, our results show an equilibrium position of $\frac{z}{h} = 0.4504$ and $\frac{z}{h} = 0.4446$ for a single particle in the straight microchannel of Newtonian fluid with $Re = 48$ and $Re = 90$, respectively, which leads to a shift of the equilibrium position toward the center of the microchannel with increasing the Re number and is in full agreement with the literature [60,61]. It can also be inferred that the equilibrium position is not a strong function of the Re number for inertial focusing in a straight microchannel of Newtonian fluids. Although the

inertial lift forces are almost zero at the center of the microchannel, this position cannot be considered a stable equilibrium position since the particle moves easily with small upward/downward forces. Starting from the center of the microchannel ($z = 0$), the particle tends to move toward its equilibrium position, so the total inertial lift force is positive (dominant region of the shear gradient lift forces). As the particle approaches its equilibrium position, the magnitude of inertial lift force becomes small. As the particle moves away from the equilibrium position to the microchannel wall, a total negative inertial lift force is exerted on the particle (dominant region of wall-induced lift forces). The magnitude of this negative lift force increases rapidly as the particle approaches the wall due to strong wall-induced lift forces. Furthermore, in agreement with the literature [62], the magnitude of the inertial lift forces decreases with increasing the Re number of the Newtonian fluid.

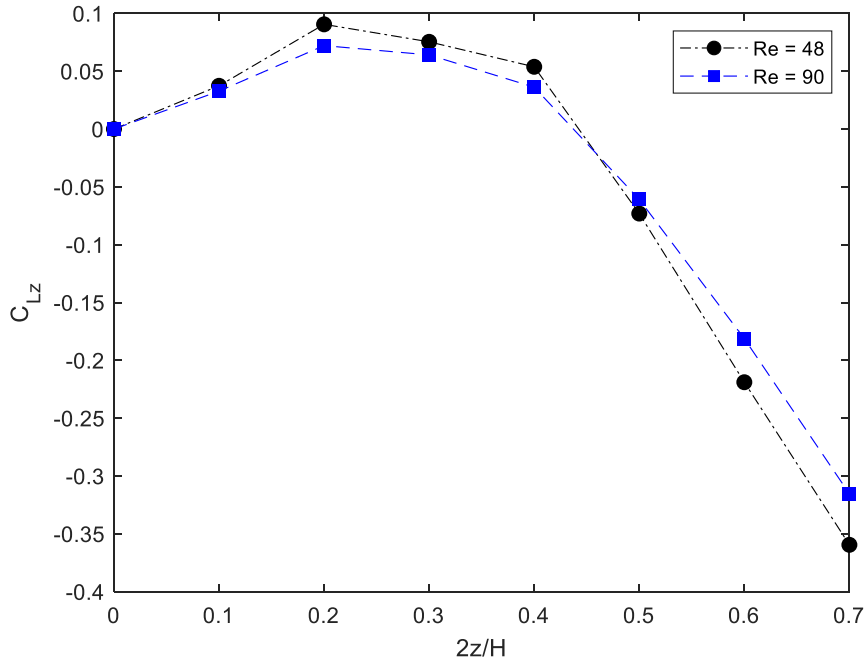

Fig. 7: Inertial lift coefficient for a particle in Newtonian fluid

The coefficients of inertial lift forces are calculated and shown in Fig. 8 as a function of the particle center position for power-law and Carreau-Yasuda representation of xanthan 300 ppm and 500 ppm solutions in two different Re numbers. As expected, the positive and negative inertial lift regions representing the dominant region of the shear gradient and the wall-induced lift forces, respectively, yield the final equilibrium position of the particle in the microchannel. Similar to the Newtonian fluid for both Re numbers, moving from the center of the microchannel toward the equilibrium position of the particle, an increase followed by a decrease in the positive inertial lift forces is observed. Additionally, moving from the particle

equilibrium position toward the microchannel wall, a sharp increase in negative inertial lift forces is observed, again similar to the Newtonian fluid. Furthermore, it can be concluded that each non-Newtonian viscosity model exerts different inertial lift forces on the particle, thus providing more control over the particle motion in the passive method of inertial microfluidics. An interesting observation is that in the power-law model, by increasing the Re number, the magnitude of inertial lift forces increases. This change in inertial lift force behavior with respect to the Re number is in contrast with that of Newtonian and Carreau-Yasuda fluids. This new pattern of behavior has been indirectly addressed by Hu [29,30] as an increase in the particle migration velocity with increasing the Re number in the power-law model and also an increase in the oscillatory amplitude of particle spacing with increasing/decreasing the Re number of the Newtonian/power-law fluid. However, this is the first time that the shift in the Re dependence of inertial lift forces in the power-law model is explicitly detected by calculating the inertial lift forces. Since the Carreau-Yasuda model assures a more accurate representation of xanthan gum viscosity (Fig. 6), the power-law model may not be a reliable model to account for the inertial focusing in shear-thinning fluids in real-world problems. Furthermore, with the exception of the power-law representation of xanthan 500 ppm (Fig. 8c), the inertial lift forces are weakly dependent on the Re number. In this case, the power-law viscosity faces a more dramatic change with respect to the shear rate (Fig. 6). As a result, even small changes in the shear rate, i.e., the Re number, lead to considerable changes in the viscosity and consequently the inertial lift forces exerted on the particle. This prediction may as well explain another drawback of the power-law model in real-world rather than mathematical representation of inertial focusing in shear-thinning fluids. In a nutshell, although the power-law model serves as a baseline for representing the shear-thinning rheology, it cannot provide an accurate representation of inertial lift forces in shear-thinning fluids. On the other hand, the Carreau-Yasuda model can accurately represent the shear-thinning rheology for the entire range of shear rates and thus generates true representation of inertial lift forces in shear-thinning fluids. The main reason behind the discrepancies between the two models lies within their viscosity differences and is explained in depth in the following.

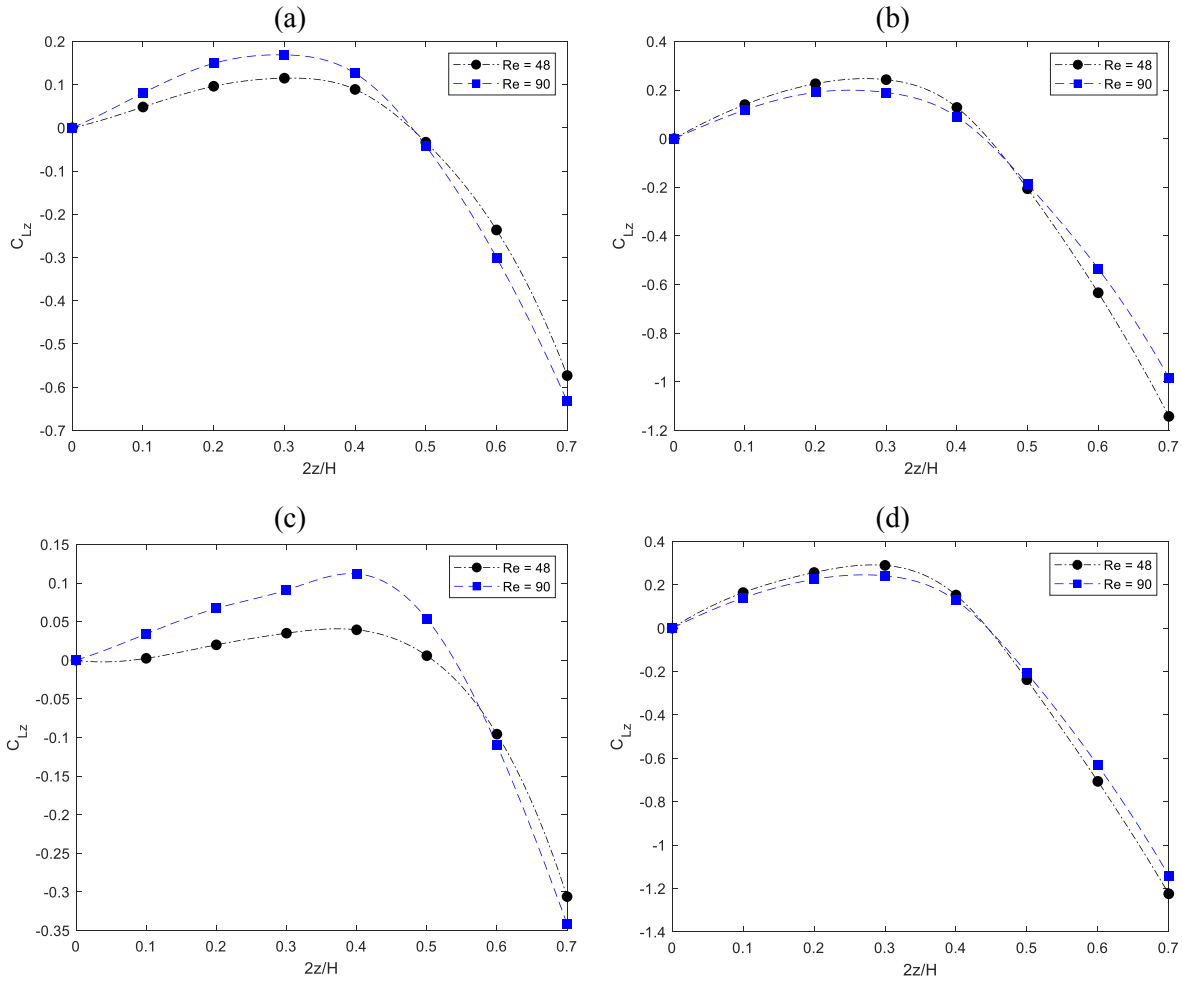

Fig. 8: Inertial lift coefficients for a particle in (a) power-law model of xanthan 300 ppm, (b) Carreau-Yasuda model of xanthan 300 ppm, (c) power-law model of xanthan 500 ppm, and (d) Carreau-Yasuda model of xanthan 500 ppm

Fig. 9 compares the coefficient of inertial lift forces exerted on the particle calculated by power-law and Carreau-Yasuda models for xanthan gum solutions in two different Re numbers. Although theoretically, the inertial lift forces are constant for a specific flow of each concentration of xanthan gum solutions, due to striking differences in the mathematical formulation of power-law and Carreau-Yasuda models, a marked discrepancy in the magnitude of the inertial lift forces is observed for the specified models, which calls for further explanations. Based on formulation, the power-law model can only represent the power-law region of the viscosity. On the other hand, the Carreau-Yasuda model can accurately represent the viscosity at the entire range of shear rate by being able to exhibit the plateau regions of the viscosity. Based on the considerable differences between the magnitude of inertial lift forces reported by the two models, we can conclude that the viscosity of the solution is a determinant factor for the inertial lift forces exerted on the particles. To elaborate that, the power-law model in the center of the microchannel cross section, i.e., the low shear-rate region, overestimates the viscosity of the xanthan gum solutions. As a result, the particle faces a high viscous medium

in the initial nodes of Fig. 9a and Fig. 9b, resulting in smaller shear gradient lift forces. In contrast, the Carreau-Yasuda model fits the viscosity of the xanthan gum solutions in the same region, resulting in higher shear gradient lift forces to traverse a less viscous medium (Fig. 9a and Fig. 9b). A similar explanation can be proposed for the wall region, i.e., the high shear-rate region. In this situation, the power-law model underestimates the viscosity which results in a low viscous medium for the particle. Thus, the positive shear gradient lift forces increase and aim to decrease the negative wall-induced lift forces. Concretely, in the wall region, smaller lift forces (in magnitude) are exerted on the particle in the power-law model compared with the Carreau-Yasuda model which does not show this underprediction of xanthan gum viscosity. Since the 500 ppm solution has a more dominant shear-thinning characteristic, the difference in the prediction of xanthan gum viscosity by the power-law and Carreau-Yasuda models becomes more noticeable, leading to a greater divergence in the prediction of the inertial lift forces by the two models (Fig. 9b).

A point which requires further elaboration is the primary factors affecting the differences between the inertial lift forces of the two viscosity models. Generally speaking, each factor which has a potential effect on the viscosity can develop discrepancies between the results of the two models. One factor which is studied is the shear-thinning characteristics. As the shear-thinning rheology becomes more dominant (for example switching from xanthan 300 ppm to xanthan 500 ppm) the degree to which the power-law model over/underestimates the viscosity increases. Consequently, the differences between the results of the two models become more noticeable. Another parameter is the Re number or the flow rate in the microchannel. This directly relates to the range of shear rate of the flow. If the Re number is in a range which mostly includes intermediate shear rates, the differences between the two models should decrease because in this region power-law viscosity and Carreau-Yasuda viscosity almost match each other. In contrast, if the Re number, i.e., the shear rate, is either in low or high regions, the inertial lift forces reported by the two models greatly differ from each other. Needless to say, all the mentioned results and predictions apply to inertial microfluidics in which the Re number is neither very small nor very large representing the importance of both inertial and viscous forces.

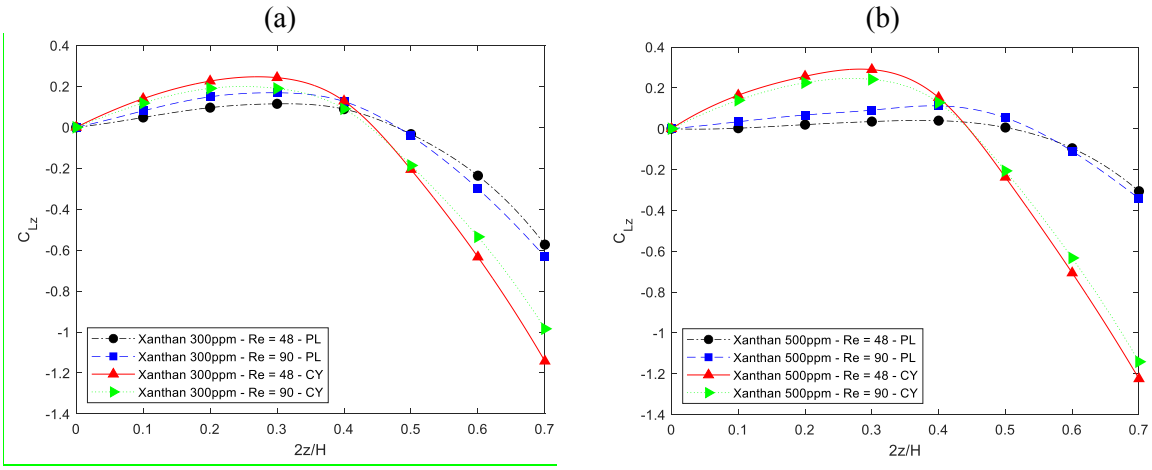

Fig. 9: Comparison between inertial lift coefficients of power-law and Carreau-Yasuda models for a particle in (a) xanthan 300 ppm and (b) xanthan 500 ppm

4.5 Equilibrium Positions

Table 5 lists the equilibrium position of the particle ($2z_{eq}/H$) in the two simulated Re numbers of Newtonian, power-law, and Carreau-Yasuda fluids. The reported values are measured from the center of the microchannel, i.e., $\frac{2z}{H} = 0$ represents the microchannel center. Due to the symmetry, each value in Table 5 expresses two equilibrium positions for the particle, one above and the other below the microchannel centerline. As mentioned earlier, the Newtonian fluid tends to push the equilibrium position of the particle toward the microchannel center by increasing the Re number. However, in the studied range of Re number, a slight movement of equilibrium position regarding the Re number is observed in the Newtonian fluid. A similar trend is detected for the xanthan gum solution as both equilibrium positions emerge across the microchannel cross-section in the studied range of Re number. The power-law model pushes the particle equilibrium position toward the microchannel wall by an increase in the Re number. On the contrary, the Carreau-Yasuda model slightly moves the particle equilibrium position toward the microchannel center by increasing the Re number. This contrast can be clarified by further exploring the combination of fluid inertia and shear thinning. In inertial focusing in rectangular microchannels, due to pure inertial forces, the particles migrate to two equilibrium positions in the short length of the microchannel cross-section by the same distance from the centerline. On the other hand, the pure shear-thinning characteristic pushes the particles toward the corners of the microchannel cross-section [39,41]. In this study, the combined effect of fluid inertia and shear thinning governs all the simulated cases. Since the power-law model exaggerates the shear-thinning characteristics compared to the Carreau-Yasuda model, the balance in the combination of inertia and shear thinning is altered from one model to another

at each Re number. Another discrepancy between the two shear-thinning models is the effect of Re number on the equilibrium positions. The Re number produces a powerful effect on the equilibrium positions in the power-law model. This result can be justified by the mathematical representation of this model. The range of Re number studied in this work creates regions of high shear rates (order of $\sim 10^4, 10^5\ s^{-1}$) in the microchannel cross section. Based on Fig. 6, in this region, the power-law model greatly underestimates the xanthan gum viscosity, especially for the higher concentration. As a result, even small changes in the shear rate, i.e., the Re number, yields unreasonable changes in the equilibrium positions of the particle. On the other hand, the Carreau-Yasuda model is insensitive to the shear rate in the mentioned range which indicates the small change of equilibrium positions in this model with respect to the Re number. However, both models can explicitly show the shift in the particle equilibrium position by changing the xanthan gum solution. Higher concentrations of xanthan gum solution move the particle equilibrium position to the microchannel wall due to stronger shear-thinning characteristics. This fact, which is proved by both power-law and Carreau-Yasuda models in our simulations, is frequently observed in the literature [29–32].

Table 5: Equilibrium position ($2z_{eq}/H$) of the particle in two Re numbers of Newtonian, power-law, and Carreau-Yasuda fluids

Re number	Newtonian	power-law		Carreau-Yasuda	
		Xanthan 300 ppm	Xanthan 500 ppm	Xanthan 300 ppm	Xanthan 500 ppm
$Re = 48$	0.4504	0.4785	0.5091	0.4447	0.4449
$Re = 90$	0.4446	0.4803	0.5409	0.4386	0.4447

4.6 Flow around the Particle

The flow around the particle is shown in Fig. 10 at a point with the coordinate of $x = 0$, $y = 0$, and $z = 14.4\ \mu m$ in the 500ppm xanthan solution and $Re = 48$. Fig. 10a to Fig. 10d and Fig. 10e to Fig. 10h are extracted from the simulations with the power-law and Carreau-Yasuda models, respectively. For all the cases, a similar trend is observed for the power-law and Carreau-Yasuda results. Fig. 10a and Fig. 10e depict the velocity profile in two different planes. Maximum velocity occurs at the wall of the microchannel, which accounts for the moving wall boundary condition. Fig. 10b and Fig. 10f show the top-view of the non-dimensional pressure $((p - p_0)/(0.5\rho\bar{V}^2))$ on the particle surface while Fig. 10d and Fig. 10h show the side-view

of the same pressure contour. The maximum and minimum pressures can be easily noticed on the particle surface. The low-pressure zone sucks the particle in while the high-pressure zone pushes it out. Similar to Newtonian fluids, in generalized Newtonian fluids, the lateral migration of the particles is governed primarily by the pressure forces rather than viscous forces [63,64]. The variation of this pressure is greater in the Carreau-Yasuda model compared to the power-law model, resulting in stronger negative wall-induced lift forces exerted on the particle for the Carreau-Yasuda model at the specified location. Although the difference in the pressure distribution on the particle surface exerts lift forces on the particle, it has no influence on the rotation of the particle. The viscous forces on the particle surface cause this rotation which results in bending the streamlines around the particle (Fig. 10c and Fig. 10g). The direction of this rotation is obtained based on the direction of the streamlines.

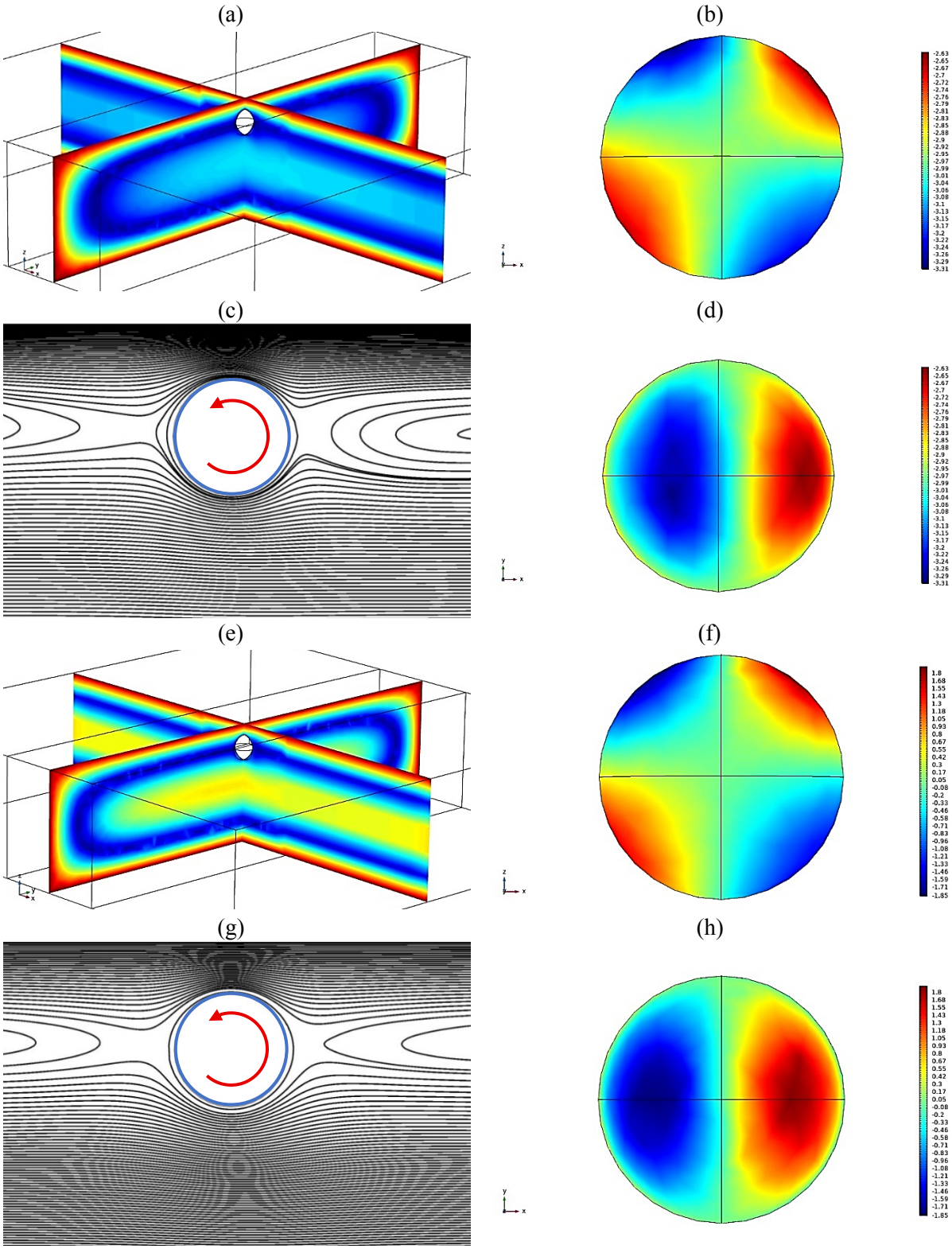

Fig. 10: Flow around the particle at $x = 0$, $y = 0$, and $z = 14.4\ \mu m$ in the 500 ppm xanthan gum solution and $Re = 48$. Figures 10(a) to 10(d) represent the power-law model while figures 10(e) to 10(h) represent the Carreau-Yasuda model. (a) and (e) Velocity profile in two planes. (b) and (f) The side-view of non-dimensional pressure on the particle surface. (c) and (g) The streamlines around the particle at $y = 0$. (d) and (h) The top-view of non-dimensional pressure on the particle surface.

5 Conclusions

In this paper, the inertial lift forces were calculated for a single particle immersed in a Newtonian fluid and two xanthan gum solutions flowing through a straight microchannel with a rectangular cross-section. An iterative algorithm that couples a FEM solver with a MATLAB code was implemented to carry out the 3D DNS of the flow around the particle. The performance of the algorithm was validated by previous results of the lift force exerted on a particle in Newtonian fluids. To capture the shear-thinning characteristics of the xanthan gum solutions, power-law and Carreau-Yasuda models were fitted to our experimental data of the xanthan gum viscosity. For all the simulations, there exist the dominant region of the shear gradient and wall-induced lift forces resulting in the emergence of two equilibrium positions. This fact demonstrates the ability of Newtonian, power-law, and Carreau-Yasuda fluids for inertial focusing of different particles. Since the power-law model overestimates and underestimates the xanthan gum viscosity in low and high shear-rate regions, respectively, the obtained inertial lift forces from this model differed considerably from those of Carreau-Yasuda model, especially for a high concentration of xanthan gum solutions. The discrepancy between the two non-Newtonian models was also observed in the Re dependency of inertial lift forces. That is, an increase in the Re number resulted in an increase and a decrease in the magnitude of inertial lift forces exerted on the particle in the power-law and the Carreau-Yasuda fluids, respectively. The equilibrium position of the particle was achieved by pinpointing the location where the inertial lift forces become zero. In full agreement with the literature [29,30,60,61,65], by increasing the Re number of the Newtonian and power-law fluids, the equilibrium position moved toward the center and the wall of the microchannel, respectively. In contrast with the power-law model, the equilibrium position moved toward the center of the microchannel in the Carreau-Yasuda model. Furthermore, the Re number appeared to be of minor importance for the final equilibrium position in Newtonian and Carreau-Yasuda fluids; however, the power-law model, especially for xanthan 500 ppm, pointed out a more noticeable effect of Re number on the final equilibrium position of the particle. This stems from the fact that, based on its definition, the power-law model is highly sensitive to the flow shear rate, i.e., the Re number, especially at high shear-rate regions due to the underprediction of viscosity. However, both models accurately represented the shift of the equilibrium position toward the microchannel wall by an increase in the shear-thinning characteristics of the fluid, a fact which was previously examined in the literature [29–32].

The results of the present study are applicable to inertial focusing and particle separation in curved microchannels as well. With the same cross-section and Re number, the inertial lift forces exerted on the particle are the same in straight and curved microchannels. Consequently, by taking into account the secondary flow drag forces and integrating the inertial lift forces into the Lagrangian tracking method, inertial focusing in curved microchannels of power-law and Carreau-Yasuda fluids can be studied as well. To the best of our knowledge, this was the first time in the literature that the inertial lift forces were directly calculated for a particle in power-law and Carreau-Yasuda fluids. Concretely, further explorations of inertial lift forces in these models are required to conclusively prove the interesting observations of the present study. Furthermore, for the sake of computational costs, only two non-Newtonian fluids at two different Re numbers were examined in our simulations. By extending the range of non-Newtonian fluids and Re number, more intriguing phenomena may emerge. Since a variety of biological fluids are non-Newtonian, the separation of biological and synthetic particles and cells in these fluids is of key importance for future studies.

Declaration of competing interest

The authors declare that they have no known competing financial interests or personal relationships that could have appeared to influence the work reported in this paper.

Data availability statement

The data that support the findings of this study are available from the corresponding author upon reasonable request.

Acknowledgements

This research did not receive any specific grant from funding agencies in the public, commercial, or not-for-profit sectors.

References

[1] A.A.S. Bhagat, H. Bow, H.W. Hou, S.J. Tan, J. Han, C.T. Lim, Microfluidics for cell separation, Med. Biol. Eng. Comput. 48 (2010) 999–1014. https://doi.org/10.1007/s11517-010-0611-4.

[2] M.E. Jun Zhanga, Sheng Yana, Dan Yuana, Gursel Alicia, Nam-Trung Nguyenb, W.L. Warkiani c, Fundamentals and Applications of Inertial Microfluidics: A Review, Lab Chip. 16 (2015) 10–34. https://doi.org/https://doi.org/10.1039/C5LC01159K.

[3] A. SEGRÉ, G., SILBERBERG, Radial Particle Displacements in Poiseuille Flow of Suspensions, Nature. 189 (1961) 209–210. https://doi.org/https://doi.org/10.1038/189209a0.

[4] J.B. McLaughlin, The lift on a small sphere in wall-bounded linear shear flows., J. Fluid Mech. 22 (1993) 385–400. https://doi.org/10.1017/S0022112093000114.

[5] P. Cherukat, J.B. McLaughlin, Corrigendum: The inertial lift on a rigid sphere in a linear shear flow field near a flat wall, J. Fluid Mech. 285 (1995) 407. https://doi.org/10.1017/S0022112095000590.

[6] E.S. Asmolov, The inertial lift on a spherical particle in a plane Poiseuille flow at large channel Reynolds number, J. Fluid Mech. 381 (1999) 63–87. https://doi.org/10.1017/S0022112098003474.

[7] D.D. Joseph, D. Ocando, Slip velocity and lift, J. Fluid Mech. 454 (2002) 263–286. https://doi.org/10.1017/S0022112001007145.

[8] B.H. Yang, J. Wang, D.D. Joseph, H.H. Hu, T.W. Pan, R. Glowinski, Migration of a sphere in tube flow, J. Fluid Mech. 540 (2005) 109–131. https://doi.org/10.1017/S0022112005005677.

[9] B. Chun, A.J.C. Ladd, Inertial migration of neutrally buoyant particles in a square duct: An investigation of multiple equilibrium positions, Phys. Fluids. 18 (2006) 1–5. https://doi.org/10.1063/1.2176587.

[10] P.G. Saffman, The lift on a small sphere in a slow shear flow, J. Fluid Mech. 22 (1965) 385–400. https://doi.org/10.1017/S0022112065000824.

[11] S.I. Rubinow, J.B. Keller, The transverse force on a spinning sphere moving in a viscous fluid, J. Fluid Mech. 11 (1961) 447–459. https://doi.org/10.1017/S0022112061000640.

[12] E. Michaelides, Particles, bubbles & drops: their motion, heat and mass transfer, World Scientific, 2006.

[13] J.P. Matas, J.F. Morris, E. Guazzelli, Lateral forces on a sphere, Oil Gas Sci. Technol. 59 (2004) 59–70. https://doi.org/10.2516/ogst:2004006.

[14] Y.S. Choi, K.W. Seo, S.J. Lee, Lateral and cross-lateral focusing of spherical particles in a square microchannel, Lab Chip. 11 (2011) 460–465. https://doi.org/10.1039/c0lc00212g.

[15] E.J. Hinch, J.A. Schonberg, Inertial migration of a sphere in Poiseuille flow, J. Fluid Mech. 203 (1989) 517–524. https://doi.org/https://doi.org/10.1017/S0022112089001564.

[16] J.B. Mclaughlin, Inertial migration of a small sphere in linear shear flows, J. Fluid Mech.

224 (1991) 261–274. https://doi.org/10.1017/S0022112091001751.

[17] K. Hood, S. Lee, M. Roper, Inertial migration of a rigid sphere in three-dimensional Poiseuille flow, J. Fluid Mech. 765 (2015) 452–479. https://doi.org/10.1017/jfm.2014.739.

[18] B.P. ho, L.G. Leal, Inertial migration of rigid spheres in two-dimensional unidirectional flows, J. Fluid Mech. 65 (1974) 365–400. https://doi.org/10.1017/S0022112074001431.

[19] D. Di Carlo, Inertial microfluidics, Lab Chip. 9 (2009) 3038–3046. https://doi.org/10.1039/b912547g.

[20] C. Liu, G. Hu, X. Jiang, J. Sun, Inertial focusing of spherical particles in rectangular microchannels over a wide range of Reynolds numbers, Lab Chip. 15 (2015) 1168–1177. https://doi.org/10.1039/c4lc01216j.

[21] G.H. Chao Liu, Chundong Xue, Jiashu Sun, A Generalized Formula for Inertial Lift on a Sphere in Microchannels, Lab Chip. 16 (2016) 884–892. https://doi.org/https://doi.org/10.1039/C5LC01522G.

[22] A. Mashhadian, A. Shamloo, Inertial microfluidics: A method for fast prediction of focusing pattern of particles in the cross section of the channel, Anal. Chim. Acta. 1083 (2019) 137–149. https://doi.org/10.1016/j.aca.2019.06.057.

[23] J. Su, X. Chen, Y. Zhu, G. Hu, Machine learning assisted fast prediction of inertial lift in microchannels, Lab Chip. 21 (2021) 2544–2556. https://doi.org/10.1039/d1lc00225b.

[24] X. Lu, C. Liu, G. Hu, X. Xuan, Particle manipulations in non-Newtonian microfluidics: A review, J. Colloid Interface Sci. 500 (2017) 182–201. https://doi.org/10.1016/j.jcis.2017.04.019.

[25] P. Wang, Z. Yu, J. Lin, Numerical simulations of particle migration in rectangular channel flow of Giesekus viscoelastic fluids, J. Nonnewton. Fluid Mech. 262 (2018) 142–148. https://doi.org/10.1016/j.jnnfm.2018.04.011.

[26] T. Fei, F. Qiang, Q. Chen, C. Liu, L. Tiejun, J. Sun, Manipulation of bio - micro / nanoparticles in non - Newtonian microflows, Microfluid. Nanofluidics. 23 (2019) 1–9. https://doi.org/10.1007/s10404-019-2232-z.

[27] A.H. Raffiee, A.M. Ardekani, S. Dabiri, Numerical investigation of elasto-inertial particle focusing patterns in viscoelastic microfluidic devices, J. Nonnewton. Fluid Mech. 272 (2019) 104166. https://doi.org/10.1016/j.jnnfm.2019.104166.

[28] E. Chaparian, M.N. Ardekani, L. Brandt, O. Tammisola, Particle migration in channel flow of an elastoviscoplastic fluid, J. Nonnewton. Fluid Mech. 284 (2020) 104376. https://doi.org/10.1016/j.jnnfm.2020.104376.

[29] X. Hu, J. Lin, X. Ku, Inertial migration of circular particles in Poiseuille flow of a power-law fluid Inertial migration of circular particles in Poiseuille flow of a power-law fluid, Phys. Fluids. 31 (2019) 73306. https://doi.org/https://doi.org/10.1063/1.5108797.

[30] X. Hu, J. Lin, D. Chen, X. Ku, Influence of non-Newtonian power law rheology on inertial migration of particles in channel flow, Biomicrofluidics. 14 (2020) 14105. https://doi.org/https://doi.org/10.1063/1.5134504.

[31] F.E. Chrit, S. Bowie, A. Alexeev, Inertial migration of spherical particles in channel

flow of power law fluids, Phys. Fluids. 32 (2020) 83103. https://doi.org/10.1063/5.0013725.

[32] X. Hu, J. Lin, Y. Guo, X. Ku, Motion and equilibrium position of elliptical and rectangular particles in a channel flow of a power-law fluid, Powder Technol. 377 (2021) 585–596. https://doi.org/10.1016/j.powtec.2020.09.028.

[33] M.G. Lee, S. Choi, J.K. Park, Rapid laminating mixer using a contraction-expansion array microchannel, Appl. Phys. Lett. 95 (2009) 97–100. https://doi.org/10.1063/1.3194137.

[34] D.H. Yoon, J.B. Ha, Y.K. Bahk, T. Arakawa, S. Shoji, J.S. Go, Size-selective separation of micro beads by utilizing secondary flow in a curved rectangular microchannel, Lab Chip. 9 (2009) 87–90. https://doi.org/10.1039/b809123d.

[35] A. Shamloo, P. Vatankhah, A. Akbari, Analyzing mixing quality in a curved centrifugal micromixer through numerical simulation, Chem. Eng. Process. - Process Intensif. 116 (2017) 9–16. https://doi.org/10.1016/j.cep.2017.03.008.

[36] A. Shamloo, A. Mashhadian, Inertial particle focusing in serpentine channels on a centrifugal platform, Phys. Fluids. 30 (2018) 12002. https://doi.org/https://doi.org/10.1063/1.5002621.

[37] S. Razavi Bazaz, A. Mashhadian, A. Ehsani, S.C. Saha, T. Krüger, M. Ebrahimi Warkiani, Computational inertial microfluidics: a review, Lab Chip. 20 (2020) 1023–1048. https://doi.org/10.1039/c9lc01022j.

[38] Y. Li, H. Zhang, Y. Li, X. Li, J. Wu, S. Qian, F. Li, Dynamic control of particle separation in deterministic lateral displacement separator with viscoelastic fluids, Sci. Rep. 8 (2018) 1–9. https://doi.org/10.1038/s41598-018-21827-7.

[39] D. Li, X. Xuan, Fluid rheological effects on particle migration in a straight rectangular microchannel, Microfluid. Nanofluidics. 22 (2018) 49. https://doi.org/https://doi.org/10.1007/s10404-018-2070-4.

[40] D. Li, X. Shao, J.B. Bostwick, X. Xuan, Particle separation in xanthan gum solutions, Microfluid. Nanofluidics. 23 (2019) 125. https://doi.org/10.1007/s10404-019-2292-0.

[41] D. Li, X. Xuan, The motion of rigid particles in the Poiseuille flow of pseudoplastic fluids through straight rectangular microchannels, Microfluid. Nanofluidics. 23 (2019) 54. https://doi.org/https://doi.org/10.1007/s10404-019-2224-z.

[42] M.K. Raihan, D. Li, A.J. Kummetz, L. Song, L. Yu, X. Xuan, Vortex trapping and separation of particles in shear thinning fluids, Appl. Phys. Lett. 116 (2020) 183701. https://doi.org/https://doi.org/10.1063/5.0008833.

[43] A. Shamloo, S. Ebrahimi, A. Amani, F. Fallah, Targeted Drug Delivery of Microbubble to Arrest Abdominal Aortic Aneurysm Development: A Simulation Study Towards Optimized Microbubble Design, Sci. Rep. 10 (2020) 1–17. https://doi.org/10.1038/s41598-020-62410-3.

[44] G. Cuvelier, B. Launay, Concentration regimes in xanthan gum solutions deduced from flow and viscoelastic properties, Carbohydr. Polym. 6 (1986) 321–333. https://doi.org/10.1016/0144-8617(86)90023-8.

[45] P.J. Whitcomb, C.W. Macosko, Rheology of Xanthan Gum, J. Rheol. (N. Y. N. Y). 22

(1978) 493–505. https://doi.org/10.1122/1.549485.

[46] K.-W. Song, Y.-S. Kim, G.-S. Chang, Rheology of concentrated xanthan gum solutions: Steady shear flow behavior, Fibers Polym. 7 (2006) 129–138.

[47] C.W. Macosko, Rheology: Principles, Measurements and Applications, Wiley, New York, 1994. https://doi.org/10.1016/s0032-5910(96)90008-x.

[48] K. Yasuda, R.C. Armstrong, R.E. Cohen, Shear flow properties of concentrated solutions of linear and star branched polystyrenes, Rheol. Acta. 178 (1981) 163–178. https://doi.org/https://doi.org/10.1007/BF01513059.

[49] K. Madlener, B. Frey, H.K. Ciezki, Generalized reynolds number for non-newtonian fluids, Prog. Propuls. Phys. 1 (2009) 237–250. https://doi.org/10.1051/eucass/200901237.

[50] J. Boyd, J.M. Buick, S. Green, Analysis of the Casson and Carreau-Yasuda non-Newtonian blood models in steady and oscillatory flows using the lattice Boltzmann method, Phys. Fluids. 19 (2007). https://doi.org/10.1063/1.2772250.

[51] T. Sochi, Analytical solutions for the flow of Carreau and Cross fluids in circular pipes and thin slits, Rheol. Acta. 54 (2015) 745–756. https://doi.org/10.1007/s00397-015-0863-x.

[52] A. Shamekhi, K. Sadeghy, Cavity flow simulation of Carreau – Yasuda non-Newtonian fluids using PIM meshfree method, Appl. Math. Model. 33 (2009) 4131–4145. https://doi.org/10.1016/j.apm.2009.02.009.

[53] G.M. de Oliveira, L.L.V. da Rocha, A.T. Franco, C.O.R. Negrão, Numerical simulation of the start-up of Bingham fluid flows in pipelines, J. Nonnewton. Fluid Mech. 165 (2010) 1114–1128. https://doi.org/10.1016/j.jnnfm.2010.05.009.

[54] A.A.S. Bhagat, S.S. Kuntaegowdanahalli, I. Papautsky, Enhanced particle filtration in straight microchannels using shear-modulated inertial migration, Phys. Fluids. 20 (2008) 1–5. https://doi.org/10.1063/1.2998844.

[55] A.A.S. Bhagat, S.S. Kuntaegowdanahalli, I. Papautsky, Inertial microfluidics for continuous particle filtration and extraction, Microfluid. Nanofluidics. 7 (2009) 217–226. https://doi.org/10.1007/s10404-008-0377-2.

[56] Z. Ouyang, J. Lin, X. Ku, The hydrodynamic behavior of a squirmer swimming in power-law fluid, Phys. Fluids. 30 (2018) 83301. https://doi.org/https://doi.org/10.1063/1.5045701.

[57] Y. Xia, J. Lin, X. Ku, Flow-induced rotation of circular cylinder in Poiseuille flow of power-law fluids, J. Nonnewton. Fluid Mech. 260 (2018) 120–132. https://doi.org/10.1016/j.jnnfm.2018.07.003.

[58] M. Yang, S. Krishnan, E.S.G. Shaqfeh, Numerical simulations of the rheology of suspensions of rigid spheres at low volume fraction in a viscoelastic fluid under shear, J. Nonnewton. Fluid Mech. 234 (2016) 51–68. https://doi.org/10.1016/j.jnnfm.2016.04.003.

[59] A. Zhang, W.L. Murch, J. Einarsson, E.S.G. Shaqfeh, Lift and drag force on a spherical particle in a viscoelastic shear flow, J. Nonnewton. Fluid Mech. 280 (2020) 104279. https://doi.org/https://doi.org/10.1016/j.jnnfm.2020.104279.

[60] M. Abbas, P. Magaud, Y. Gao, S. Geoffroy, Migration of finite sized particles in a laminar square channel flow from low to high Reynolds numbers, Phys. Fluids. 26 (2014) 123301. https://doi.org/https://doi.org/10.1063/1.4902952.

[61] H. Shichi, H. Yamashita, J. Seki, T. Itano, M. Sugihara-Seki, Inertial migration regimes of spherical particles suspended in square tube flows, Phys. Rev. Fluids. 2 (2017) 1–12. https://doi.org/10.1103/PhysRevFluids.2.044201.

[62] Q. Wang, D. Yuan, W. Li, Analysis of hydrodynamic mechanism on particles focusing in micro-channel flows, Micromachines. 8 (2017) 197. https://doi.org/https://doi.org/10.3390/mi8070197.

[63] J. Feng, H.H. Hu, D.D. Joseph, Direct simulation of initial value problems for the motion of solid bodies in a Newtonian fluid, Part 1. Sedimentation, J. Fluid Mech. 261 (1994) 95–134. https://doi.org/https://doi.org/10.1017/S0022112094000285.

[64] L. Zeng, S. Balachandar, P. Fischer, Wall-induced forces on a rigid sphere at finite Reynolds number, J. Fluid Mech. 536 (2005) 1–25. https://doi.org/10.1017/S0022112005004738.

[65] D.M. Nie, J.Z. Lin, Behavior of three circular particles in a confined power-law fluid under shear, J. Nonnewton. Fluid Mech. 221 (2015) 76–94. https://doi.org/10.1016/j.jnnfm.2015.04.004.